



Time-harmonic Green's function and boundary integral formulation for incremental nonlinear elasticity: dynamics of wave patterns and shear bands

Davide Bigoni^{a,*}, Domenico Capuani^b

^a*Dipartimento di Ingegneria Meccanica e Strutturale, Università di Trento, Via Mesiano 77,
38050 Povo, Trento, Italy*

^b*Dipartimento di Architettura, Università di Ferrara, Via Quartieri 8, 44100 Ferrara, Italy*

Received 3 June 2004; received in revised form 22 November 2004; accepted 24 November 2004

Abstract

Superimposed dynamic, time-harmonic incremental deformations are considered in an elastic, orthotropic and incompressible, infinite body, subject to plane, homogeneous—but otherwise arbitrary—deformation. The dynamic, infinite body Green's function is found and, in addition, new boundary integral equations are obtained for incremental in-plane hydrostatic stress and displacements. These findings open the way to integral methods in incremental, dynamic elasticity. Moreover, the Green's function is employed as a dynamic perturbation to analyze interaction between wave propagation and shear band formation. Depending on anisotropy and pre-stress level, peculiar wave patterns emerge with focussing and shadowing effects of signals, which may remain undetected by the usual criteria based on analysis of weak discontinuity surfaces.

© 2005 Elsevier Ltd. All rights reserved.

Keywords: Dynamic Green's function; Boundary integral equations; Nonlinear elasticity; Shear bands; Boundary element method; Wave propagation; Pre-stressed media; Anisotropy

*Corresponding author. Tel.: +39 0461 882507; fax: +39 0461 882599.

E-mail addresses: bigoni@ing.unitn.it (D. Bigoni), cpd@unife.it (D. Capuani).

1. Introduction

FINDINGS by Bigoni and Capuani (2002) pertaining to quasi-static deformation of pre-stressed, elastic orthotropic and incompressible materials are extended in the present article to the dynamic, time-harmonic regime. In particular, infinite-body, dynamic *Green's functions* and *boundary integral equations* for incremental displacements and in-plane incremental hydrostatic stress, are obtained for small-isochoric and two-dimensional-deformation superimposed upon a given nonlinear elastic and homogeneous strain. Due to the hypothesis of time-harmonic deformation, the regime classification of the governing differential equations remains identical to the quasi-static case, so that all obtained solutions lie within the elliptic range. A perturbation in terms of a pulsating dipole can be therefore obtained and employed to analyze material instabilities arising near the boundary of ellipticity loss. The perturbative approach is *general*—since it can be employed for any incrementally linear constitutive equation, dynamic loadings and inhomogeneous material (Willis, 1991)—and is capable of *revealing aspects which may remain undetected* using methods for material instabilities based on weak discontinuity surfaces (loss of ellipticity, e.g. Knowles and Sternberg, 1978). For instance, the perturbative approach has revealed shear band formation for a Mooney–Rivlin material in the quasi-static case (Bigoni and Capuani, 2002, their Fig. 3), a circumstance confirmed by the present dynamic analysis, but not detected by the conventional approach.

Results presented in this article provide a basis for the analysis of propagation of dynamic disturbances near the boundary of loss of ellipticity. Depending on the level of pre-stress and anisotropy, wave patterns are shown to emerge, with focussing of signals in the direction of shear bands. Varying the direction of the dynamic perturbation excites different wave patterns, which tend to degenerate to families of plane waves parallel to the shear bands, when the elliptic boundary is approached.

Another possibility related to the finding of a Green's function is the formulation of a boundary element technique for the solution of incremental boundary value problems. For quasi-static deformation, this technique was proved to possess certain advantages—related for instance to the treatment of the incompressibility constraint—with respect to other numerical techniques, such as finite-element methods (Brun et al., 2003a, b). Now the development of the technique in dynamics requires the finding of new boundary integral equations. While the integral equation for incremental displacements does not formally change with respect to the quasi-static case, a generalization is given of the integral representation for incremental in-plane hydrostatic stress obtained by Bigoni and Capuani (2002).

The paper is organized as follows. After a brief presentation of the constitutive framework (Section 2), the dynamic Green's function set, composed of incremental displacements (Eq. (31)), and in-plane incremental hydrostatic stress (Eq. (40)), is obtained in Section 3. Wave patterns produced by a dynamic perturbation at different pre-stress levels are analyzed in Section 4 and, finally, boundary integral equations for incremental displacement (Eq. (43)), and in-plane incremental hydrostatic stress (Eq. (54)), are given in Section 5.

2. Constitutive framework

We refer to the two-dimensional [Biot \(1965\)](#) constitutive framework detailed in [Bigoni and Capuani \(2002\)](#) and [Brun et al. \(2003a\)](#). In the principal reference system of Cauchy stress (here denoted by in-plane indices 1 and 2) and using a Lagrangean formulation of the field equations with the current state taken as reference, the constitutive relation can be written as

$$\dot{t}_{ij} = \mathbb{K}_{ijkl} v_{l,k} + \dot{p} \delta_{ij}, \quad (1)$$

where¹ \dot{t}_{ij} is the increment of nominal stress t_{ij} , induced by the gradient of incremental displacement v_i through the fourth-order tensor \mathbb{K}_{ijkl} and, independently, by the in-plane hydrostatic stress increment \dot{p} . Note that tensor \mathbb{K}_{ijkl} possesses the major symmetry, $\mathbb{K}_{ijkl} = \mathbb{K}_{klij}$ and is a function of the principal components of Cauchy stress σ_1 and σ_2 , describing the pre-stress, and of two incremental moduli μ and μ_* (which can depend arbitrarily on the current stress and strain). It is defined by the following non-null components:

$$\begin{aligned} \mathbb{K}_{1111} &= \mu_* - \frac{\sigma}{2} - p, & \mathbb{K}_{1122} &= \mathbb{K}_{2211} = -\mu_*, & \mathbb{K}_{2222} &= \mu_* + \frac{\sigma}{2} - p, \\ \mathbb{K}_{1212} &= \mu + \frac{\sigma}{2}, & \mathbb{K}_{1221} &= \mathbb{K}_{2112} = \mu - p, & \mathbb{K}_{2121} &= \mu - \frac{\sigma}{2} \end{aligned} \quad (2)$$

with

$$\sigma = \sigma_1 - \sigma_2, \quad p = \frac{\sigma_1 + \sigma_2}{2}. \quad (3)$$

The constitutive equations (1) are complemented by the incompressibility constraint

$$v_{i,i} = 0. \quad (4)$$

Constitutive equations (1)–(4) describe a broad class of material behaviors, including all possible elastic incompressible materials isotropic in an initial state ([Biot, 1965](#); [Brun et al., 2003a](#)), but also materials which are *orthotropic* with respect to the current principal stress directions (1 and 2). The latter situation has interesting practical applications in the field of fiber-reinforced elastic materials. Here, loss of ellipticity may explain occurrence of different failure modes, such as fiber kinking, splitting and debonding ([Merodio and Pence, 2001](#); [Merodio and Ogden, 2002](#)). In particular, the constitutive framework given by [Merodio and Pence \(2001\)](#) and [Merodio and Ogden \(2002\)](#) can be given the format employed in the present paper when the principal components of current stress are aligned normal and parallel to the fibers. In the following, no specific assumptions will be made on the dependence of μ_* and μ on the current state.

¹The standard, indicial notation employed by [Bigoni and Capuani \(2002\)](#) is used throughout this paper, where a comma denotes partial differentiation, repeated indices are summed (between 1 and 2) and δ_{ij} is the Kronecker delta. Superposed dot denotes an incremental quantity.

3. The dynamic Green’s function set

Superimposed incremental deformations upon a homogeneously pre-deformed infinite medium are considered, produced by application of a time-harmonic point load acting at the point $\mathbf{x} = \mathbf{0}$ and with components $\dot{f}_1(t), \dot{f}_2(t)$ at time t , along the principal stress axes. While the current state of stress trivially satisfies equilibrium, the equations of motion for superimposed disturbances are

$$\dot{i}_{ij,i} + \dot{f}_j \delta(\mathbf{x}) = \rho v_{j,t}, \tag{5}$$

where δ is the two-dimensional Dirac delta function and ${}_t$ denotes the material time derivative. In the hypothesis of time-harmonic motion with circular frequency Ω , every field $g(\mathbf{x}, t)$ can be expressed as $g(\mathbf{x})e^{-i\Omega t}$ and Eq. (5) becomes

$$\begin{aligned} (2\mu_* - \mu)v_{1,11} + \left(\mu - \frac{\sigma}{2}\right)v_{1,22} + \dot{f}_1 \delta(\mathbf{x}) &= -\dot{\pi}_{,1} - \rho\Omega^2 v_1, \\ (2\mu_* - \mu)v_{2,22} + \left(\mu + \frac{\sigma}{2}\right)v_{2,11} + \dot{f}_2 \delta(\mathbf{x}) &= -\dot{\pi}_{,2} - \rho\Omega^2 v_2, \end{aligned} \tag{6}$$

where

$$\dot{\pi} = \frac{\dot{i}_{11} + \dot{i}_{22}}{2} = \dot{p} - \frac{\sigma}{2} v_{1,1} \tag{7}$$

is the increment of in-plane nominal hydrostatic stress. Note that, due to the time-harmonic assumption, Eqs. (6) are independent of time.

Introducing the stream function $\psi(x_1, x_2)$ as

$$v_1 = \psi_{,2}, \quad v_2 = -\psi_{,1} \tag{8}$$

and the dimensionless pre-stress parameter

$$k = \frac{\sigma}{2\mu}. \tag{9}$$

Eqs. (6)₁ and (6)₂ can be combined to give

$$\begin{aligned} (1+k)\psi_{,1111} + 2\left(2\frac{\mu_*}{\mu} - 1\right)\psi_{,1122} + (1-k)\psi_{,2222} + \frac{\dot{f}_1}{\mu} \delta_{,2} - \frac{\dot{f}_2}{\mu} \delta_{,1} \\ = -\frac{\rho\Omega^2}{\mu}(\psi_{,11} + \psi_{,22}). \end{aligned} \tag{10}$$

It is important to realize now that, since only the principal part of a differential operator plays a role in determining the regime classification (see for instance [Renardy and Rogers, 1993](#)), the classification of Eq. (10) remains the same as for the quasi-static case.

Since the classification of governing differential equations does not change from the quasi-static case, we remark that all results in this paper will be restricted to the

elliptic regime, defined through the condition that scalars γ_1 and γ_2 :

$$\left. \begin{matrix} \gamma_1 \\ \gamma_2 \end{matrix} \right\} = \frac{1 - 2\mu_*/\mu \pm \sqrt{\Delta}}{1 + k}, \quad \Delta = k^2 - 4 \frac{\mu_*}{\mu} + 4 \left(\frac{\mu_*}{\mu} \right)^2, \tag{11}$$

are either both real and negative in the elliptic imaginary regime (EI) or a conjugate pair in the elliptic complex regime (EC). Note that Δ is positive in (EI) and negative in (EC).

A consequence of the above discussion is that the emergence of weakly discontinuous surfaces corresponds in the present context to failure of ellipticity, as in the quasi-static case. This occurs in a continuous loading path (starting from E) either when $k = 1$ (so that $\gamma_1 = 0$) or when $\Delta = 0$ (so that $\gamma_1 = \gamma_2$). The former case defines the elliptic-imaginary/parabolic boundary, while the latter the elliptic-complex/hyperbolic boundary.

3.1. The dynamic Green’s function for incremental displacements

Taking $\dot{f}_i = \delta_{ig}$, Eq. (10) can be rewritten as

$$\mu \mathcal{L} \psi^g + \left(\delta_{1g} \frac{\partial \cdot}{\partial x_2} - \delta_{2g} \frac{\partial \cdot}{\partial x_1} \right) \delta(\mathbf{x}) = -\rho \Omega^2 \nabla^2 \psi^g, \tag{12}$$

where ∇^2 is the Laplacian and \mathcal{L} is the linear differential operator defined as

$$\mathcal{L}(\cdot) = (1 + k) \frac{\partial^4 \cdot}{\partial x_1^4} + 2 \left(2 \frac{\mu_*}{\mu} - 1 \right) \frac{\partial^4 \cdot}{\partial x_1^2 \partial x_2^2} + (1 - k) \frac{\partial^4 \cdot}{\partial x_2^4}. \tag{13}$$

We follow here the procedure used by [Bigoni and Capuani \(2002\)](#) of employing plane wave expansions of the functions involved ([Gel’fand and Shilov, 1964](#); see [Willis, 1973](#), for applications in elasticity). In particular, the plane wave expansions of the δ function and of the stream function $\psi^g(\mathbf{x})$ are

$$\delta(\mathbf{x}) = -\frac{1}{4\pi^2} \oint_{|\boldsymbol{\omega}|=1} \frac{d\boldsymbol{\omega}}{(\boldsymbol{\omega} \cdot \mathbf{x})^2}, \quad \psi^g(\mathbf{x}) = -\frac{1}{4\pi^2} \oint_{|\boldsymbol{\omega}|=1} \tilde{\psi}^g(\boldsymbol{\omega} \cdot \mathbf{x}) d\boldsymbol{\omega}, \tag{14}$$

where $\boldsymbol{\omega}$ is a unit vector. Substituting representations (14) into Eq. (12) yields

$$(\tilde{\psi}^g)'''' + \frac{\rho \Omega^2}{L(\boldsymbol{\omega})} (\tilde{\psi}^g)'' = 2 \frac{\delta_{1g} \omega_2 - \delta_{2g} \omega_1}{L(\boldsymbol{\omega})(\boldsymbol{\omega} \cdot \mathbf{x})^3}, \tag{15}$$

where a prime denotes differentiation with respect to the variable $\boldsymbol{\omega} \cdot \mathbf{x}$ and

$$L(\boldsymbol{\omega}) = \mu \omega_2^4 (1 + k) \left[\frac{\omega_1^2}{\omega_2^2} - \gamma_1 \right] \left[\frac{\omega_1^2}{\omega_2^2} - \gamma_2 \right] > 0. \tag{16}$$

Note that the velocity of a transverse plane wave propagating in the direction defined by the unit vector $\boldsymbol{\omega}$ is $[L(\boldsymbol{\omega})/\rho]^{1/2}$.

The integral of differential equation (15) with respect to the variable $\boldsymbol{\omega} \cdot \mathbf{x}$ can be obtained through variation of parameters in the form

$$\begin{aligned} \tilde{\psi}^g(\boldsymbol{\omega} \cdot \mathbf{x}) = & \frac{(\delta_{1g}\omega_2 - \delta_{2g}\omega_1)}{\Omega\sqrt{\rho L(\boldsymbol{\omega})}} \{ \text{Ci}(\eta|\boldsymbol{\omega} \cdot \mathbf{x}|) \sin(\eta\boldsymbol{\omega} \cdot \mathbf{x}) - \text{Si}(\eta\boldsymbol{\omega} \cdot \mathbf{x}) \cos(\eta\boldsymbol{\omega} \cdot \mathbf{x}) \\ & + A_1 \sin(\eta\boldsymbol{\omega} \cdot \mathbf{x}) + A_2 \cos(\eta\boldsymbol{\omega} \cdot \mathbf{x}) + i[A_3 \sin(\eta\boldsymbol{\omega} \cdot \mathbf{x}) + A_4 \cos(\eta\boldsymbol{\omega} \cdot \mathbf{x})] \}, \end{aligned} \tag{17}$$

where A_j ($j = 1, \dots, 4$) are arbitrary constants, $i = \sqrt{-1}$, η is the wave-number (in the direction $\boldsymbol{\omega}$)

$$\eta = \Omega \sqrt{\frac{\rho}{L(\boldsymbol{\omega})}} \tag{18}$$

and Ci and Si are the cosine integral and sine integral functions defined as

$$\text{Si}(x) = \int_0^x \frac{\sin t}{t} dt, \quad \text{Ci}(x) = \gamma + \log x + \int_0^x \frac{\cos t - 1}{t} dt, \tag{19}$$

where $\gamma \cong 0.577216$ is the Euler Gamma constant.

To determine now constants A_j in Eq. (17), let us consider the far-field approximation in the variable $\boldsymbol{\omega} \cdot \mathbf{x}$ of the following term:

$$\begin{aligned} \text{Ci}(\eta\boldsymbol{\omega} \cdot \mathbf{x}) \sin(\eta\boldsymbol{\omega} \cdot \mathbf{x}) - \text{Si}(\eta\boldsymbol{\omega} \cdot \mathbf{x}) \cos(\eta\boldsymbol{\omega} \cdot \mathbf{x}) = & -\frac{\pi}{2} \cos(\eta\boldsymbol{\omega} \cdot \mathbf{x}) + O\left(\frac{1}{\boldsymbol{\omega} \cdot \mathbf{x}}\right), \\ (\boldsymbol{\omega} \cdot \mathbf{x} \rightarrow +\infty). \end{aligned} \tag{20}$$

Neglecting an arbitrary harmonic solution, from Eqs. (17) and (20) we get the far-field approximation for $\tilde{\psi}^g$

$$\tilde{\psi}^g(\boldsymbol{\omega} \cdot \mathbf{x}) = -\frac{(\delta_{1g}\omega_2 - \delta_{2g}\omega_1)}{\sqrt{\rho\Omega^2 L(\boldsymbol{\omega})}} \left[\frac{\pi}{2} \cos(\eta\boldsymbol{\omega} \cdot \mathbf{x}) + i \frac{\pi}{2} \sin(\eta\boldsymbol{\omega} \cdot \mathbf{x}) \right] + O\left(\frac{1}{\boldsymbol{\omega} \cdot \mathbf{x}}\right) \tag{21}$$

which features only outgoing waves.

As a consequence of asymptotic representation (21), constants A_j remain determinate and Eq. (17) becomes

$$\begin{aligned} \tilde{\psi}^g(\boldsymbol{\omega} \cdot \mathbf{x}) = & \frac{(\delta_{1g}\omega_2 - \delta_{2g}\omega_1)}{\sqrt{\rho\Omega^2 L(\boldsymbol{\omega})}} \left[\text{Ci}(\eta|\boldsymbol{\omega} \cdot \mathbf{x}|) \sin(\eta\boldsymbol{\omega} \cdot \mathbf{x}) \right. \\ & \left. - \text{Si}(\eta\boldsymbol{\omega} \cdot \mathbf{x}) \cos(\eta\boldsymbol{\omega} \cdot \mathbf{x}) - i \frac{\pi}{2} \sin(\eta\boldsymbol{\omega} \cdot \mathbf{x}) \right]. \end{aligned} \tag{22}$$

Introducing the polar coordinates $r = |\mathbf{x}|$ and ϑ of the generic point, a substitution of Eq. (22) into the plane wave expansion (14)₂ provides the *stream function*

$$\psi^g(r, \vartheta) = -\frac{1}{2\pi^2 \rho \Omega c} \int_0^\pi \frac{\sin(\alpha + \vartheta + (1-g)\pi/2)}{A(\alpha + \vartheta)} \Xi \left(\frac{\Omega r}{c} \frac{\cos \alpha}{\sqrt{A(\alpha + \vartheta)}} \right) d\alpha, \tag{23}$$

where

$$\Xi(x) = \sin x \operatorname{Ci}(|x|) - \cos x \operatorname{Si}(x) - i \frac{\pi}{2} \sin x. \tag{24}$$

Consistently with Eq. (16), the function Λ in Eq. (23) is defined as

$$\Lambda(\alpha) = \sin^4 \alpha [\cot^2 \alpha - \gamma_1][\cot^2 \alpha - \gamma_2] > 0 \tag{25}$$

and

$$c = \sqrt{\frac{\mu(1+k)}{\rho}}, \tag{26}$$

is the propagation speed of a transverse wave travelling parallel to x_1 -axis whereas

$$c\sqrt{\Lambda(\alpha)} \tag{27}$$

is the velocity of propagation in the direction singled out by angle α .

Note that the stream function (23) is *not* singular at $r = 0$ and it depends on ϑ and the dimensionless variable $\Omega r/c$.

Use of Eq. (8) allows us to introduce now the infinite body Green’s function for incremental displacements

$$v_1^g = \psi_{,2}^g, \quad v_2^g = -\psi_{,1}^g, \tag{28}$$

so that we get from Eqs. (22) and (28)

$$\begin{aligned} \tilde{v}_j^g(\boldsymbol{\omega} \cdot \mathbf{x}) = & \frac{(\delta_{1j}\omega_2 - \delta_{2j}\omega_1)(\delta_{1g}\omega_2 - \delta_{2g}\omega_1)}{L(\boldsymbol{\omega})} \left[\operatorname{Ci}(\eta|\boldsymbol{\omega} \cdot \mathbf{x}|) \cos(\eta\boldsymbol{\omega} \cdot \mathbf{x}) \right. \\ & \left. + \operatorname{Si}(\eta\boldsymbol{\omega} \cdot \mathbf{x}) \sin(\eta\boldsymbol{\omega} \cdot \mathbf{x}) - i \frac{\pi}{2} \cos(\eta\boldsymbol{\omega} \cdot \mathbf{x}) \right] \end{aligned} \tag{29}$$

which yields the Green’s tensor using

$$v_j^g(\mathbf{x}) = -\frac{1}{4\pi^2} \oint_{|\boldsymbol{\omega}|=1} \tilde{v}_j^g(\boldsymbol{\omega} \cdot \mathbf{x}) \, d\boldsymbol{\omega}. \tag{30}$$

In conclusion, the components of the Green’s tensor (30) become

$$\begin{aligned} v_1^1(r, \vartheta) = & -\frac{1}{2\pi^2\mu(1+k)} \left[\left(\log\left(\frac{\Omega r}{c}\right) + \gamma \right) \int_0^\pi \frac{\sin^2(\alpha + \vartheta)}{\Lambda(\alpha + \vartheta)} \right. \\ & \times \cos\left(\frac{\Omega r}{c} \frac{\cos \alpha}{\sqrt{\Lambda(\alpha + \vartheta)}}\right) d\alpha \\ & + \int_0^{\pi/2} \log\left(\frac{\cos \alpha}{\sqrt{\Lambda(\alpha + \vartheta)}}\right) \frac{\sin^2(\alpha + \vartheta)}{\Lambda(\alpha + \vartheta)} \\ & \left. \times \cos\left(\frac{\Omega r}{c} \frac{\cos \alpha}{\sqrt{\Lambda(\alpha + \vartheta)}}\right) d\alpha + \int_0^{\pi/2} \log\left(\frac{\sin \alpha}{\sqrt{\Lambda(\alpha + \vartheta + \pi/2)}}\right) \right] \end{aligned}$$

$$\begin{aligned} & \times \frac{\cos^2(\alpha + \vartheta)}{\Lambda(\alpha + \vartheta + \pi/2)} \cos\left(\frac{\Omega r}{c} \frac{\sin \alpha}{\sqrt{\Lambda(\alpha + \vartheta + \pi/2)}}\right) d\alpha \\ & + \int_0^\pi \frac{\sin^2(\alpha + \vartheta)}{\Lambda(\alpha + \vartheta)} \Im\left(\frac{\Omega r}{c} \frac{\cos \alpha}{\sqrt{\Lambda(\alpha + \vartheta)}}\right) d\alpha \\ & - i \frac{\pi}{2} \int_0^\pi \frac{\sin^2(\alpha + \vartheta)}{\Lambda(\alpha + \vartheta)} \cos\left(\frac{\Omega r}{c} \frac{\cos \alpha}{\sqrt{\Lambda(\alpha + \vartheta)}}\right) d\alpha \Big], \end{aligned}$$

$$\begin{aligned} v_2^2(r, \vartheta) = & -\frac{1}{2\pi^2\mu(1+k)} \left[\left(\log\left(\frac{\Omega r}{c}\right) + \gamma \right) \int_0^\pi \frac{\cos^2(\alpha + \vartheta)}{\Lambda(\alpha + \vartheta)} \right. \\ & \times \cos\left(\frac{\Omega r}{c} \frac{\cos \alpha}{\sqrt{\Lambda(\alpha + \vartheta)}}\right) d\alpha + \int_0^{\pi/2} \log\left(\frac{\cos \alpha}{\sqrt{\Lambda(\alpha + \vartheta)}}\right) \\ & \times \frac{\cos^2(\alpha + \vartheta)}{\Lambda(\alpha + \vartheta)} \cos\left(\frac{\Omega r}{c} \frac{\cos \alpha}{\sqrt{\Lambda(\alpha + \vartheta)}}\right) d\alpha \\ & + \int_0^{\pi/2} \log\left(\frac{\sin \alpha}{\sqrt{\Lambda(\alpha + \vartheta + \pi/2)}}\right) \frac{\sin^2(\alpha + \vartheta)}{\Lambda(\alpha + \vartheta + \pi/2)} \\ & \times \cos\left(\frac{\Omega r}{c} \frac{\sin \alpha}{\sqrt{\Lambda(\alpha + \vartheta + \pi/2)}}\right) d\alpha \\ & + \int_0^\pi \frac{\cos^2(\alpha + \vartheta)}{\Lambda(\alpha + \vartheta)} \Im\left(\frac{\Omega r}{c} \frac{\cos \alpha}{\sqrt{\Lambda(\alpha + \vartheta)}}\right) d\alpha, \\ & \left. - i \frac{\pi}{2} \int_0^\pi \frac{\cos^2(\alpha + \vartheta)}{\Lambda(\alpha + \vartheta)} \cos\left(\frac{\Omega r}{c} \frac{\cos \alpha}{\sqrt{\Lambda(\alpha + \vartheta)}}\right) d\alpha \right], \end{aligned} \tag{31}$$

$$\begin{aligned} v_2^1(r, \vartheta) = & -\frac{1}{2\pi^2\mu(1+k)} \\ & \times \left[- \left(\log\left(\frac{\Omega r}{c}\right) + \gamma \right) \int_0^\pi \frac{\sin(\alpha + \vartheta) \cos(\alpha + \vartheta)}{\Lambda(\alpha + \vartheta)} \right. \\ & \times \cos\left(\frac{\Omega r}{c} \frac{\cos \alpha}{\sqrt{\Lambda(\alpha + \vartheta)}}\right) d\alpha - \int_0^{\pi/2} \log\left(\frac{\cos \alpha}{\sqrt{\Lambda(\alpha + \vartheta)}}\right) \\ & \times \frac{\sin(\alpha + \vartheta) \cos(\alpha + \vartheta)}{\Lambda(\alpha + \vartheta)} \cos\left(\frac{\Omega r}{c} \frac{\cos \alpha}{\sqrt{\Lambda(\alpha + \vartheta)}}\right) d\alpha \\ & \left. + \int_0^{\pi/2} \log\left(\frac{\sin \alpha}{\sqrt{\Lambda(\alpha + \vartheta + \pi/2)}}\right) \frac{\sin(\alpha + \vartheta) \cos(\alpha + \vartheta)}{\Lambda(\alpha + \vartheta + \pi/2)} \right] \end{aligned}$$

$$\begin{aligned} & \times \cos \left(\frac{\Omega r}{c} \frac{\sin \alpha}{\sqrt{A(\alpha + \vartheta + \pi/2)}} \right) d\alpha \\ & - \int_0^\pi \frac{\sin(\alpha + \vartheta) \cos(\alpha + \vartheta)}{A(\alpha + \vartheta)} \Im \left(\frac{\Omega r}{c} \frac{\cos \alpha}{\sqrt{A(\alpha + \vartheta)}} \right) d\alpha \\ & + i \frac{\pi}{2} \int_0^\pi \frac{\sin(\alpha + \vartheta) \cos(\alpha + \vartheta)}{A(\alpha + \vartheta)} \cos \left(\frac{\Omega r}{c} \frac{\cos \alpha}{\sqrt{A(\alpha + \vartheta)}} \right) d\alpha \Big], \end{aligned}$$

where $v_2^1 = v_1^2$ (since $\tilde{v}_2^1 = \tilde{v}_1^2$ from Eq. (29)) and

$$\Im(x) = \cos x \int_0^x \frac{\cos t - 1}{t} dt + \sin x \operatorname{Si}(x) \tag{32}$$

which is *not* singular at $x = 0$.

It can be observed from Eqs. (31) that the incremental displacement has a logarithmic singularity, when $\Omega r/c$ tends to zero. Therefore, near the singularity, $r \rightarrow 0$, the asymptotic behavior of the dynamic Green’s function is identical to the quasi-static case.

3.2. The dynamic Green’s function for in-plane incremental hydrostatic stress

To complete the Green’s function set, the in-plane incremental hydrostatic stress still needs to be determined. Differentiating Eq. (6)₁ with respect to x_1 , Eq. (6)₂ with respect to x_2 and summing the results gives

$$\dot{\pi}_{,11} + \dot{\pi}_{,22} = -2(\mu_* - \mu)(v_{1,111} + v_{2,222}) + \frac{\sigma}{2}(v_{1,111} - v_{2,222}) - \dot{f}_1 \delta_{,1} - \dot{f}_2 \delta_{,2} \tag{33}$$

which is identical to the quasi-static case. Therefore, following the same arguments employed in the quasi-static case we arrive at

$$\tilde{\pi}^g(\boldsymbol{\omega} \cdot \mathbf{x}) = -2(\mu_* - \mu) [\omega_1^3 (\tilde{v}_1^g)' + \omega_2^3 (\tilde{v}_2^g)'] + \frac{\sigma}{2} [\omega_1^3 (\tilde{v}_1^g)' - \omega_2^3 (\tilde{v}_2^g)'] + \frac{\omega_g}{\boldsymbol{\omega} \cdot \mathbf{x}}, \tag{34}$$

where the Green’s incremental displacement is given by Eq. (29), so that

$$(\tilde{v}_i^g)' = \frac{\delta_{ig} - \omega_i \omega_g}{L(\boldsymbol{\omega})} \left[\frac{1}{\boldsymbol{\omega} \cdot \mathbf{x}} - \eta \Xi(\eta \boldsymbol{\omega} \cdot \mathbf{x}) \right] \tag{35}$$

with function Ξ given by Eq. (24). Employing Eq. (35) into Eq. (34) yields

$$\begin{aligned} \tilde{\pi}^g(\boldsymbol{\omega} \cdot \mathbf{x}) &= \frac{\omega_g}{\boldsymbol{\omega} \cdot \mathbf{x}} + (2g - 3) \frac{\omega_g(1 - \omega_g^2)}{L(\boldsymbol{\omega})} \left[2(\mu_* - \mu)(\omega_1^2 - \omega_2^2) - \frac{\sigma}{2} \right] \\ &\times \left[\frac{1}{\boldsymbol{\omega} \cdot \mathbf{x}} - \eta \Xi(\eta \boldsymbol{\omega} \cdot \mathbf{x}) \right]. \end{aligned} \tag{36}$$

The plane wave expansion

$$\dot{\pi}^g(\mathbf{x}) = -\frac{1}{4\pi^2} \oint_{|\boldsymbol{\omega}|=1} \tilde{\pi}^g(\boldsymbol{\omega} \cdot \mathbf{x}) d\boldsymbol{\omega}, \tag{37}$$

applied to Eq. (36) finally yields the Green’s function for the in-plane incremental hydrostatic stress

$$\begin{aligned} \dot{\pi}^1(r, \vartheta) &= (\dot{\pi}^1)_{\text{static}}(r, \vartheta) - \frac{\Omega}{2\pi^2(1+k)c} \\ &\quad \times \int_0^\pi \frac{\sin^2(\alpha + \vartheta) \cos(\alpha + \vartheta)}{A^{3/2}(\alpha + \vartheta)} \Gamma(\alpha + \vartheta) \Xi \left(\frac{\Omega r}{c} \frac{\cos \alpha}{\sqrt{A(\alpha + \vartheta)}} \right) d\alpha, \\ \dot{\pi}^2(r, \vartheta) &= (\dot{\pi}^2)_{\text{static}}(r, \vartheta) + \frac{\Omega}{2\pi^2(1+k)c} \\ &\quad \times \int_0^\pi \frac{\cos^2(\alpha + \vartheta) \sin(\alpha + \vartheta)}{A^{3/2}(\alpha + \vartheta)} \Gamma(\alpha + \vartheta) \Xi \left(\frac{\Omega r}{c} \frac{\cos \alpha}{\sqrt{A(\alpha + \vartheta)}} \right) d\alpha, \end{aligned} \tag{38}$$

where

$$\Gamma(\alpha) = 2 \left(\frac{\mu_*}{\mu} - 1 \right) (2\cos^2\alpha - 1) - k, \tag{39}$$

the integrals are non-singular functions of r and $(\cdot)_{\text{static}}$ identifies the Green’s function of the quasi-static problem

$$\begin{aligned} (\dot{\pi}^1)_{\text{static}} &= -\frac{\cos \vartheta}{2\pi r} + \frac{1}{2\pi^2 r(1+k)} \int_0^\pi \frac{1}{\cos \alpha} \left(\frac{\sin^2(\alpha + \vartheta) \cos(\alpha + \vartheta) \Gamma(\alpha + \vartheta)}{A(\alpha + \vartheta)} \right. \\ &\quad \left. + \frac{\cos^2 \vartheta \sin \vartheta \Gamma(\vartheta + \pi/2)}{A(\vartheta + \pi/2)} \right) d\alpha, \\ (\dot{\pi}^2)_{\text{static}} &= -\frac{\sin \vartheta}{2\pi r} - \frac{1}{2\pi^2 r(1+k)} \int_0^\pi \frac{1}{\cos \alpha} \left(\frac{\sin(\alpha + \vartheta) \cos^2(\alpha + \vartheta) \Gamma(\alpha + \vartheta)}{A(\alpha + \vartheta)} \right. \\ &\quad \left. - \frac{\cos \vartheta \sin^2 \vartheta \Gamma(\vartheta + \pi/2)}{A(\vartheta + \pi/2)} \right) d\alpha. \end{aligned} \tag{40}$$

It may be important to notice that the Green incremental hydrostatic stress (Eq. (38)) reduces to the quasi-static case both in the low-frequency limit and in the isotropic case, $\mu = \mu_*$, $k = 0$, the latter corresponding to $\Gamma(\alpha) = 0$.

4. Wave propagation and shear bands

Employing self-equilibrated combinations of concentrated forces, [Bigoni and Capuani \(2002\)](#) provided a perturbative approach to material instability analyzed within the boundary of loss of ellipticity. In particular, the simplest perturbing system was employed, consisting of a dipole (two equal and opposite forces), acting on a pre-stressed, infinite medium. This approach is general, so that it applies to any

incrementally linear constitutive equation² and allows for investigation of situations, such as inhomogeneous materials or dynamic loadings, where instability criteria based on weakly discontinuous surface may be in a sense “opaque”. As examples of such situations, we may mention the cases of Mooney–Rivlin, which will be confirmed here to display shear band pattern formation for dynamic disturbances, and of flutter instability, a situation which may occur when the constitutive equations lack major symmetry (which is not the case considered in this paper, but is analyzed by Piccolroaz et al. (2005)) and which remains unexplored using the conventional approach.

Similarly to the quasi-static case, a time-harmonic pulsating dipole is used as a perturbing agent, acting on a pre-stressed infinite medium. The effect of the dynamic perturbation decays with distance, but the decay becomes slower and slower in a path (in the k vs. μ_*/μ space) towards the boundary of ellipticity. The interesting feature is represented by the deformation patterns emerging when the loss of ellipticity is approached.

We begin with the simple example of a Mooney–Rivlin material (in our case of plane strain deformation this material model coincides with a neo-Hookean material) for which

$$\sigma = \mu_0(\lambda^2 - \lambda^{-2}), \quad \mu_* = \mu = \frac{\mu_0}{2}(\lambda^2 + \lambda^{-2}), \quad k = \frac{\lambda^4 - 1}{\lambda^4 + 1}, \quad (41)$$

where $\lambda > 1$ is the maximum current stretch and μ_0 is a shear modulus in an initial state. Ellipticity would be lost in the above material when $k = 1$, corresponding to the unphysical situation of infinite stretch (see Eq. (41)₃). For this material, shear band formation in the sense of emergence of discontinuity surfaces remains excluded.

Level sets of the modulus of the real (left in the figure) and imaginary (right in the figure) parts of the Green’s function for incremental displacements (Eq. (31) non-dimensionalized through multiplication by μ) are represented in the figures, in a region defined by the non-dimensional coordinates x_1/a and x_2/a , where $2a$ is the distance between two unit forces defining the dipole. Unless otherwise specified, the dipole is centred at the origin and aligned parallel to the x_1 -axis. Figs. 1–3, pertaining to Mooney–Rivlin material, are relative to different values of the pre-stress parameter k . In particular, $k = 0$ (or $\lambda = 1$ from Eq. (41)₃), for Fig. 1; $k = 0.5$ (or $\lambda \cong 1.316$ from Eq. (41)₃), for Fig. 2; and $k = 0.98$ (or $\lambda \cong 3.154$ from Eq. (41)₃), for Fig. 3.

In the quasi-static case, the displacement maps plotted in the dimensionless coordinates x_1/a and x_2/a become independent of the dipole distance a . This is not true in the dynamic case: the solution now depends on the *dimensionless*

²In classical elastoplasticity, the constitutive equations are incrementally piecewise linear and some care should be used in adopting the perturbation criterion suggested in this paper. Roughly speaking, the perturbation should be superimposed on a uniform incremental field capable of “compensating” for the possible elastic unloading which may occur near the perturbation itself (see Bigoni and Petryk, 2002, for a related discussion).

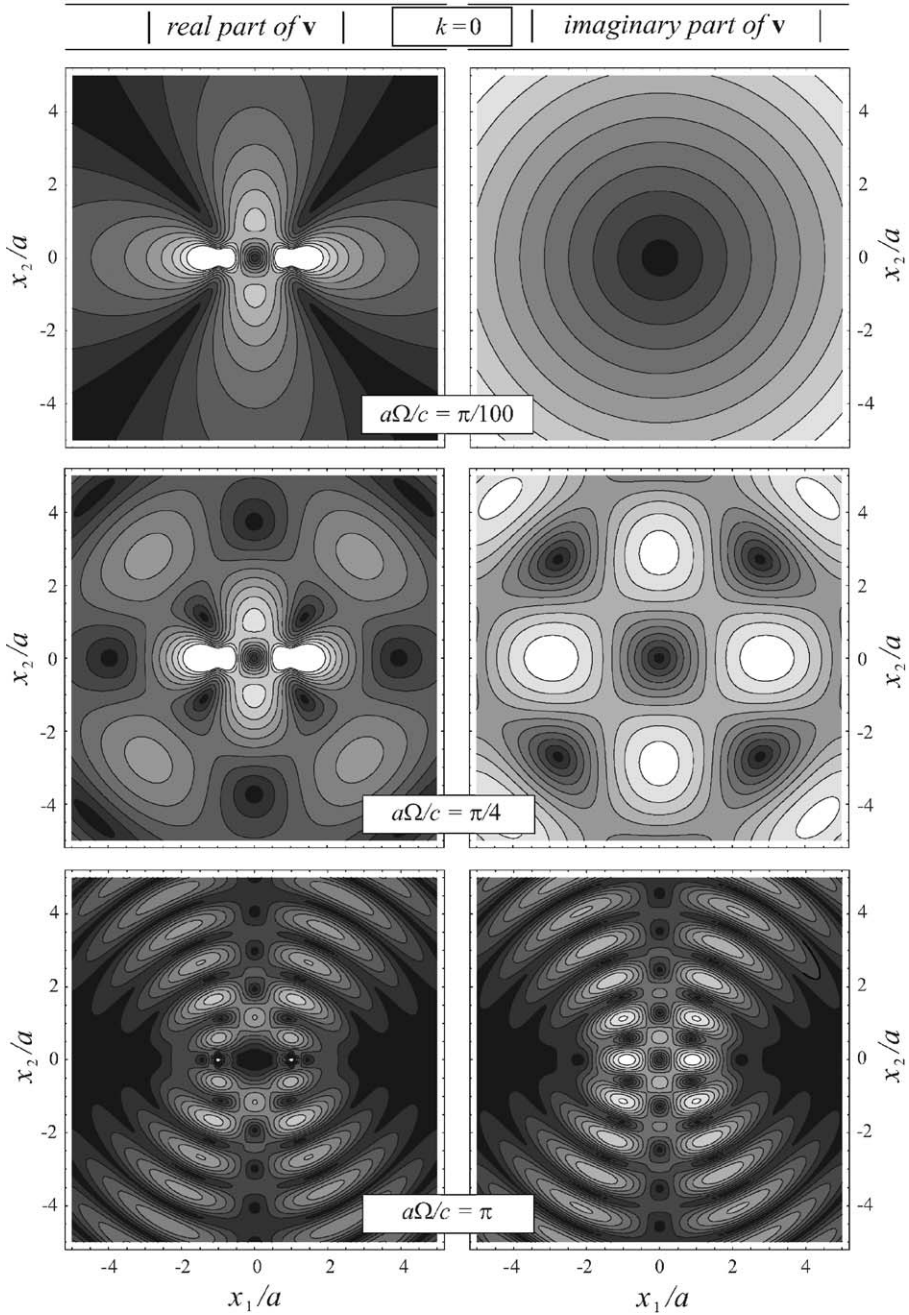


Fig. 1. Level sets of the modulus of the real part (left) and imaginary part (right) of incremental displacement, for a time-harmonic pulsating dipole aligned with the x_1 -axis. A Mooney–Rivlin material is considered, with null pre-stress, $k = 0$. Effects of varying the frequency parameter $a\Omega/c$ are shown: low frequency $a\Omega/c = \pi/100$ (upper part), $a\Omega/c = \pi/4$ (central part) and high frequency $a\Omega/c = \pi$ (lower part).

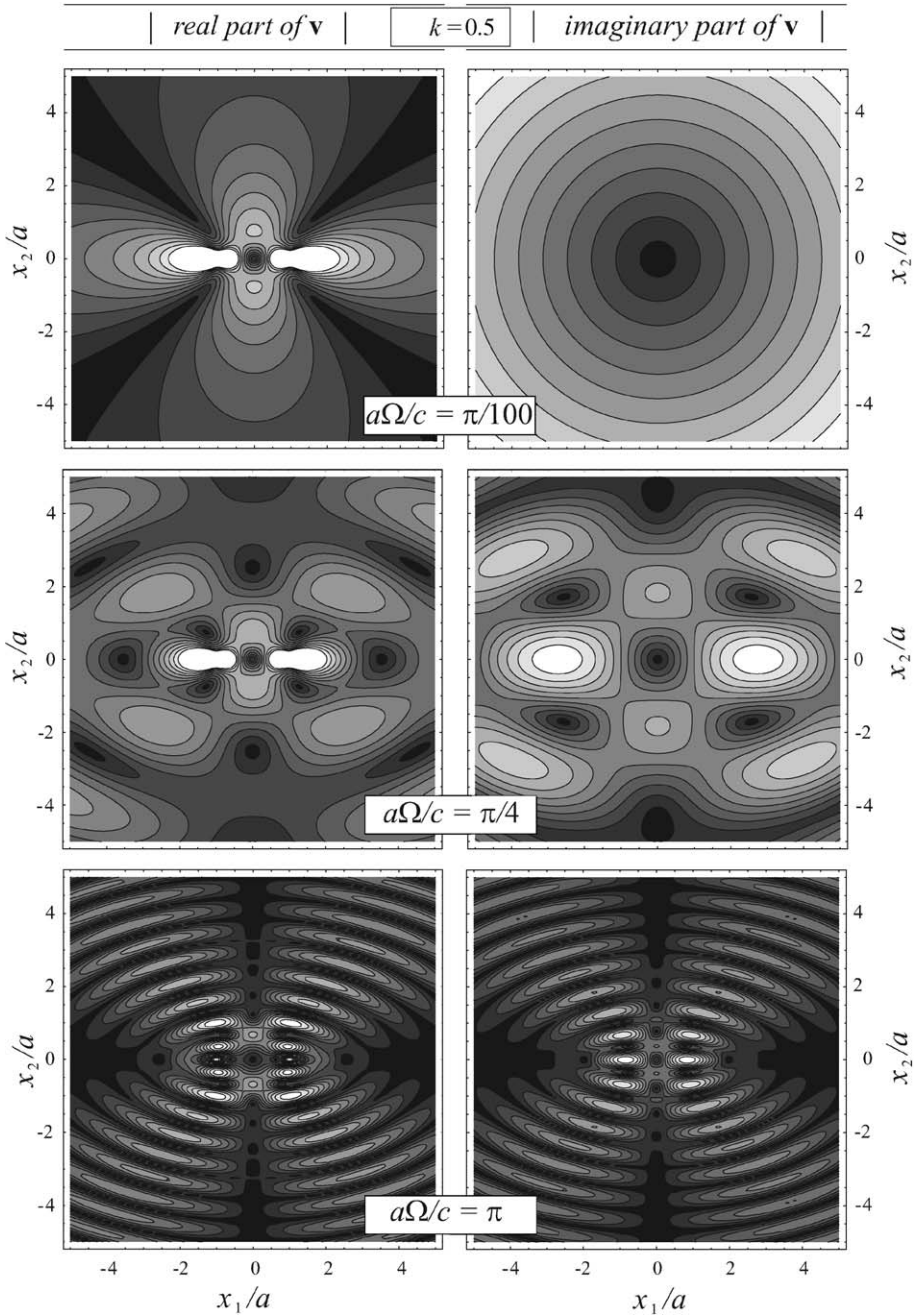


Fig. 2. Level sets of the modulus of the real part (left) and imaginary part (right) of incremental displacement, for a time-harmonic pulsating dipole aligned with the x_1 -axis. A Mooney–Rivlin material is considered, with a pre-stress $k=0.5$, corresponding to a stretch $\lambda=1.316$. Effects of varying the frequency parameter $a\Omega/c$ are shown: low frequency $a\Omega/c = \pi/100$ (upper part), $a\Omega/c = \pi/4$ (central part) and high frequency $a\Omega/c = \pi$ (lower part).

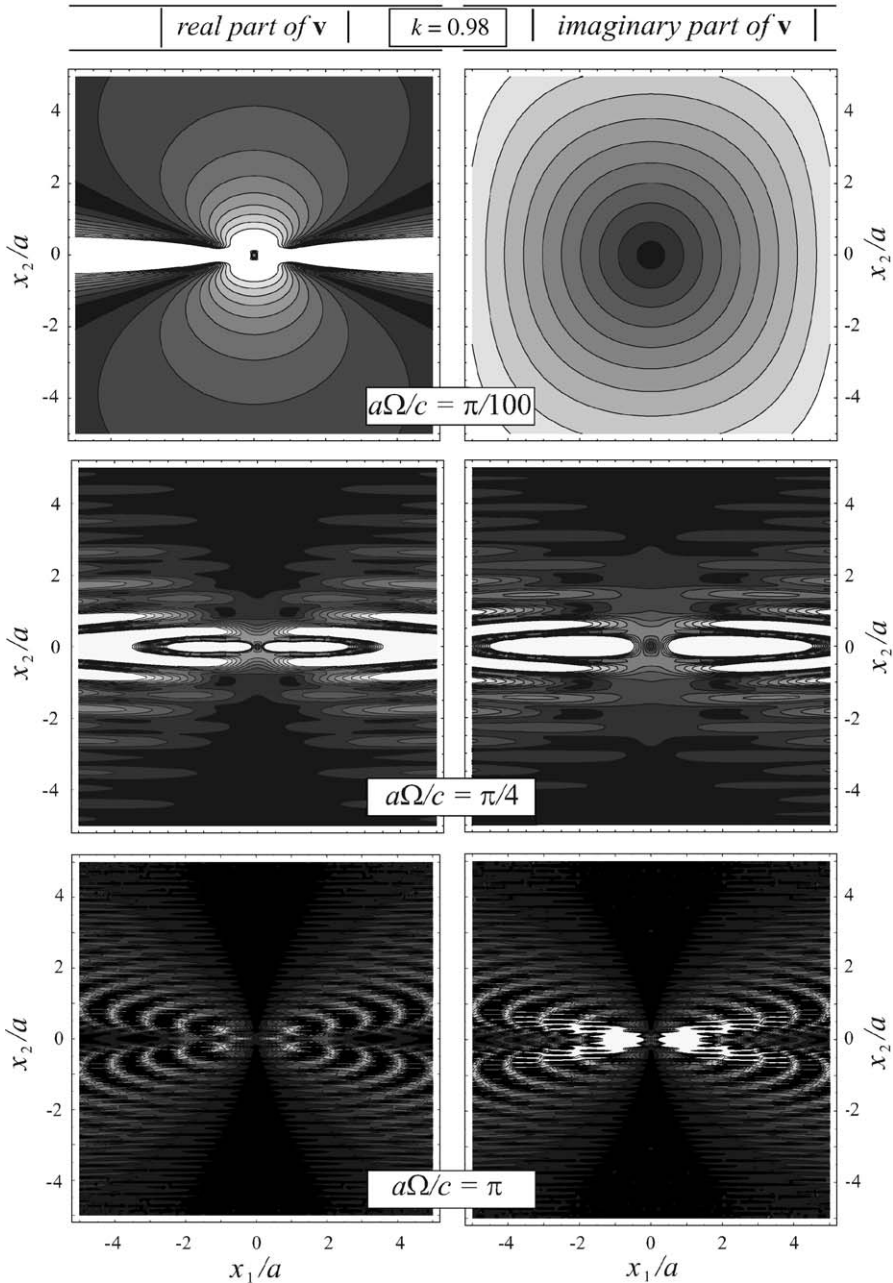


Fig. 3. Level sets of the modulus of the real part (left) and imaginary part (right) of incremental displacement, for a time-harmonic pulsating dipole aligned with the x_1 -axis. A Mooney–Rivlin material is considered, with a pre-stress $k = 0.98$, corresponding to a stretch $\lambda = 3.154$, so that the material is near the elliptic boundary. Effects of varying the frequency parameter $a\Omega/c$ are shown: low frequency $a\Omega/c = \pi/100$ (upper part), $a\Omega/c = \pi/4$ (central part) and high frequency $a\Omega/c = \pi$ (lower part). Localized deformations are evident.

scale parameter

$$\frac{a\Omega}{c} = \frac{a2\pi}{\lambda_1}, \quad (42)$$

where λ_1 corresponds to the wavelength of a plane wave propagating parallel to the x_1 -axis. Therefore, parameter (42) can be viewed as a measure of the perturbation wavelength related to the distance between the two forces forming the dipole.

The effects related to the changes in parameter (42) are systematically investigated, so that different parts of the same figures correspond (unless otherwise specified) to different values of the parameter. In particular, all upper parts of Figs. 1–3 refer to a low frequency limit, $a\Omega/c = \pi/100$, so that the real part is coincident with the quasi-static solution reported by Bigoni and Capuani (2002, their Fig. 3). The central parts of the figures correspond to $a\Omega/c = \pi/4$ and the lower parts to $a\Omega/c = \pi$. Compared to Fig. 1, we note anisotropy effects in Fig. 2, where shear banding is not yet visible. However, the anisotropy dramatically affects the propagation in Fig. 3, where $k = 0.98$, a value relatively close to the loss of ellipticity. Here shear band emergence interacts with wave propagation, creating a strong orientation (shear bands become horizontal at the EI boundary) and focussing of the signal, which tends to propagate only in the horizontal direction. The effect increases with frequency, so that at $a\Omega/c = \pi$, the width of shear bands becomes so narrow that the definition of the plot is not sufficient to visualize displacement patterns, at least at the same scale of the other figures. In this case, the signal almost does not propagate and therefore the displacement map remains prevalingly dark. Specifically, according to Eq. (27), the propagation speeds in a Mooney–Rivlin material (41) for plane waves travelling parallel to axes x_1 and x_2 are $\lambda(\mu_0/\rho)^{1/2}$ and $(\mu_0/\rho)^{1/2}/\lambda$, respectively. The former tends to infinity and the latter to zero when the elliptic boundary is approached. In the particular case of $a\Omega/c = \pi/4$ and $k = 0.98$, the wavelengths characterizing propagation parallel to axes x_1 and x_2 are $8a$ and $0.80a$, respectively. The wavelength in the direction x_2 is visible in the central part of Fig. 3 (where distance between peaks corresponds to one half of the wavelengths), whereas those along x_1 -axis become visible in Fig. 4, which is an extension of Fig. 3 with x_1/a ranging between 0 and 20. This figure shows that wave patterns emanating from the dipole have an elliptical shape, whose aspect ratio depends on the pre-stress parameter k . At increasing distance from the dipole, the disturbances tend to propagate as plane waves travelling parallel to the x_2 -axis. Moreover, the elliptical shapes tend to self-similarly decrease for increasing values of $a\Omega/c$, thus explaining the “shadowing effect” visible in the lower part of Fig. 3.

An anisotropic material with $\mu_*/\mu = 1/4$ (in which failure of ellipticity occurs at $k = 0.866$) is considered in Figs. 5–8. The parameter k is now equal to 0 in Fig. 5, which therefore corresponds to a orthotropic, incompressible material in the framework of the usual infinitesimal theory of elasticity. We note that the effect of anisotropy is pretty evident, but it is remarkably different from the situation near the boundary of loss of ellipticity, where the signal becomes localized in narrow “channels”. These are evident in Fig. 7 (corresponding to $k = 0.860$), with inclination ($\pm 27.367^\circ$) corresponding to shear bands occurring at failure of

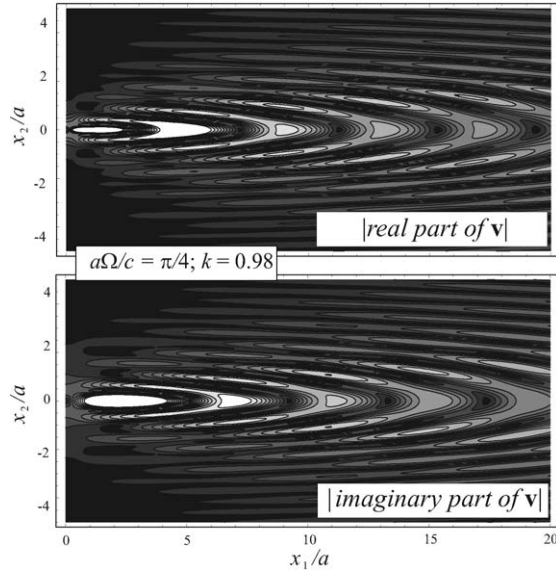


Fig. 4. Level sets of the modulus of the real part (upper part) and imaginary part (lower part) of incremental displacement, for a time-harmonic pulsating dipole aligned with the x_1 -axis. A Mooney–Rivlin material is considered, as in the central part of Fig. 3: $k = 0.98$ and $a\Omega/c = \pi/4$. The region $x_1/a \in [0, 20]$ and $x_2/a \in [-5, 5]$ is considered.

ellipticity. Fig. 6 pertains to the “intermediate” case of $k = 0.4$, where the pre-stress affects the anisotropy of the material, but is still insufficient to trigger phenomena like those evidenced near the elliptic boundary. Far from the dipole, the texture observed in the lower parts of Figs. 5 and 6 is generated by the intersection of two families of inclined wave patterns. Further, we note that, while results relative to $a\Omega/c = \pi/100$, $\pi/4$ and π are reported in Figs. 5 and 6, the value $a\Omega/c = \pi/6$ is considered in Fig. 7 instead of π since in this case the “shadowing effect” prevails and almost nothing is visualized at the same scale of the other figures.

Investigation of the effects related to possible inclinations of the dipole with respect to the principal stress reference system, also reveals interesting features (Fig. 8). We limit the present discussion to examples pertaining to a dipole aligned parallel ($\beta = 27.367^\circ$, Fig. 8 upper part) and orthogonal ($\beta = 62.633^\circ$, Fig. 8 lower part) to the shear band that would occur at the elliptic boundary. The quasi-static counterpart in the low-frequency limit may be found in Bigoni and Capuani (2002, their Fig. 7)). The frequency parameter $a\Omega/c$ has been selected here equal to $\pi/8$ (upper part of the figures). It is interesting to note that a single family of plane waves is generated in Fig. 8 (lower part), so that vibration tends to become focussed into parallel layers.

Although restricted to plane, incompressible elasticity, it is considered unlikely that the above conclusions are specific to the assumed constitutive model. Rather, we

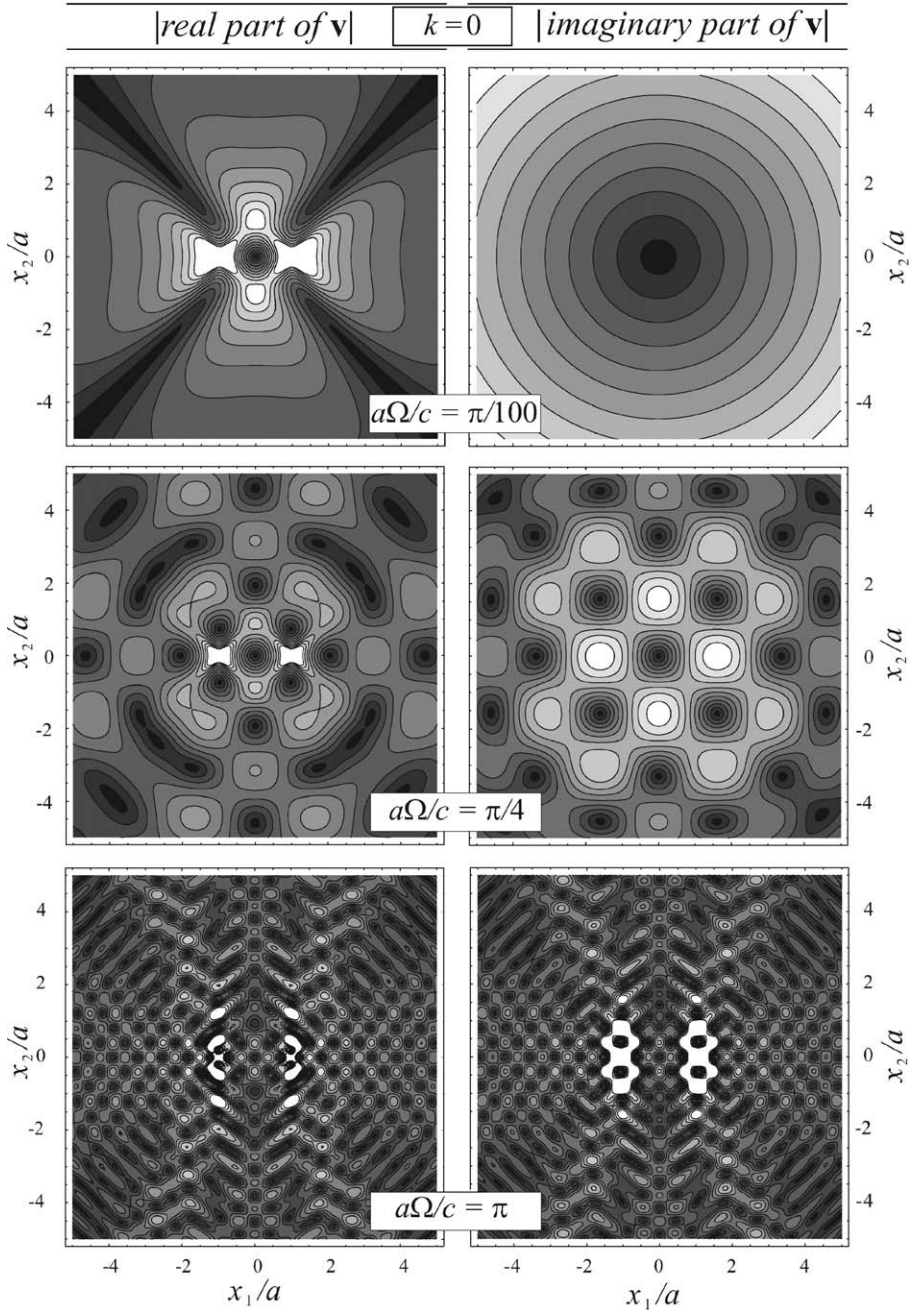


Fig. 5. Level sets of the modulus of the real part (left) and imaginary part (right) of incremental displacement, for a time-harmonic pulsating dipole aligned with the x_1 -axis. An anisotropic material with $\mu_*/\mu = 1/4$ and null pre-stress $k = 0$ is considered. Effects of varying the frequency parameter $a\Omega/c$ are shown: low frequency $a\Omega/c = \pi/100$ (upper part), $a\Omega/c = \pi/4$ (central part) and high frequency $a\Omega/c = \pi$ (lower part).

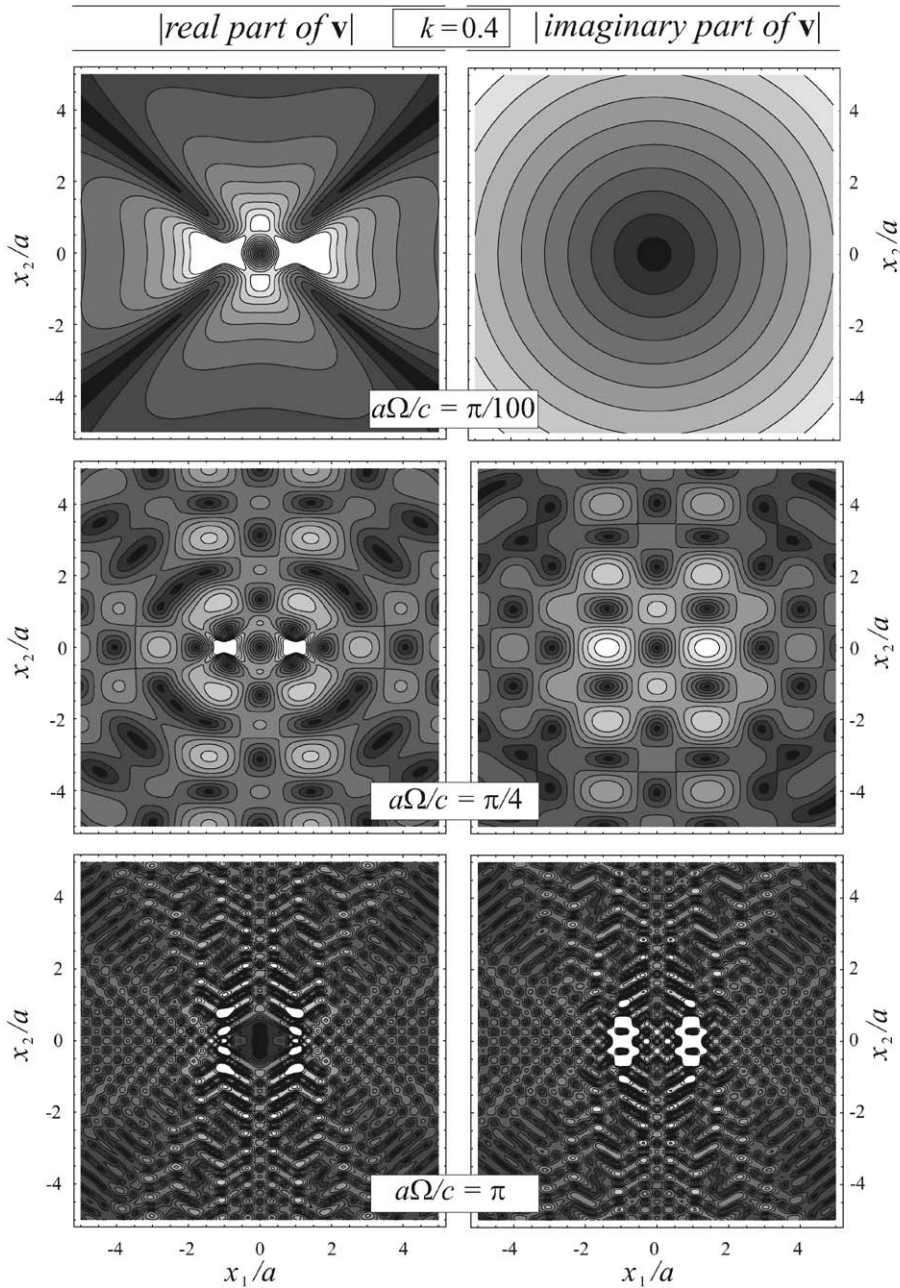


Fig. 6. Level sets of the modulus of the real part (left) and imaginary part (right) of incremental displacement, for a time-harmonic pulsating dipole aligned with the x_1 -axis. An anisotropic material with $\mu_*/\mu = 1/4$ and a pre-stress $k = 0.4$ is considered. Effects of varying the frequency parameter $a\Omega/c$ are shown: low frequency $a\Omega/c = \pi/100$ (upper part), $a\Omega/c = \pi/4$ (central part) and high frequency $a\Omega/c = \pi$ (lower part).

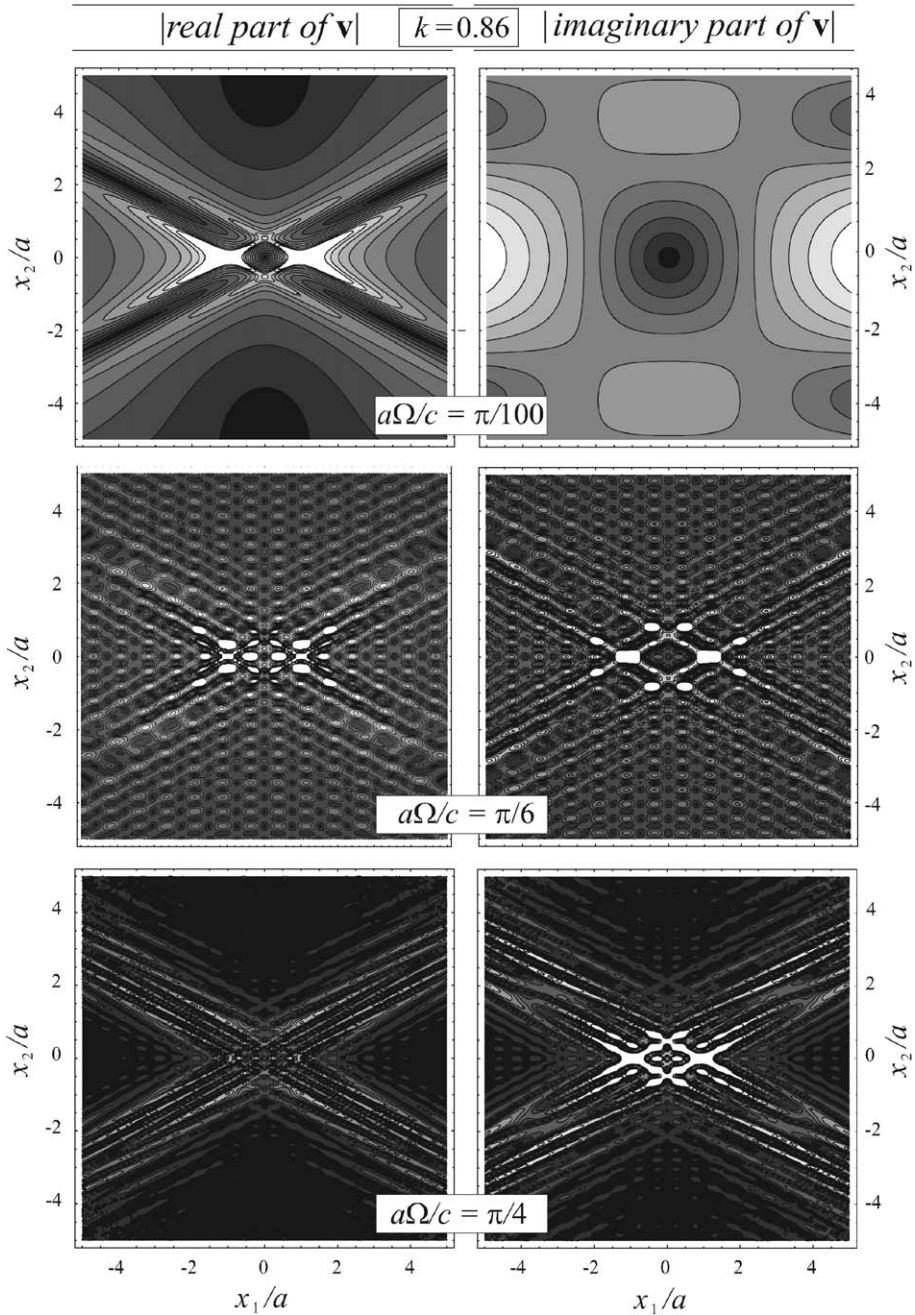


Fig. 7. Level sets of the modulus of the real part (left) and imaginary part (right) of incremental displacement, for a time-harmonic pulsating dipole aligned with the x_1 -axis. An anisotropic material with $\mu_*/\mu = 1/4$ and a pre-stress $k = 0.86$ is considered near the boundary of ellipticity. Effects of varying the frequency parameter $a\Omega/c$ are shown: low frequency $a\Omega/c = \pi/100$ (upper part), $a\Omega/c = \pi/6$ (central part) and high frequency $a\Omega/c = \pi/4$ (lower part). Localized deformations are evident.

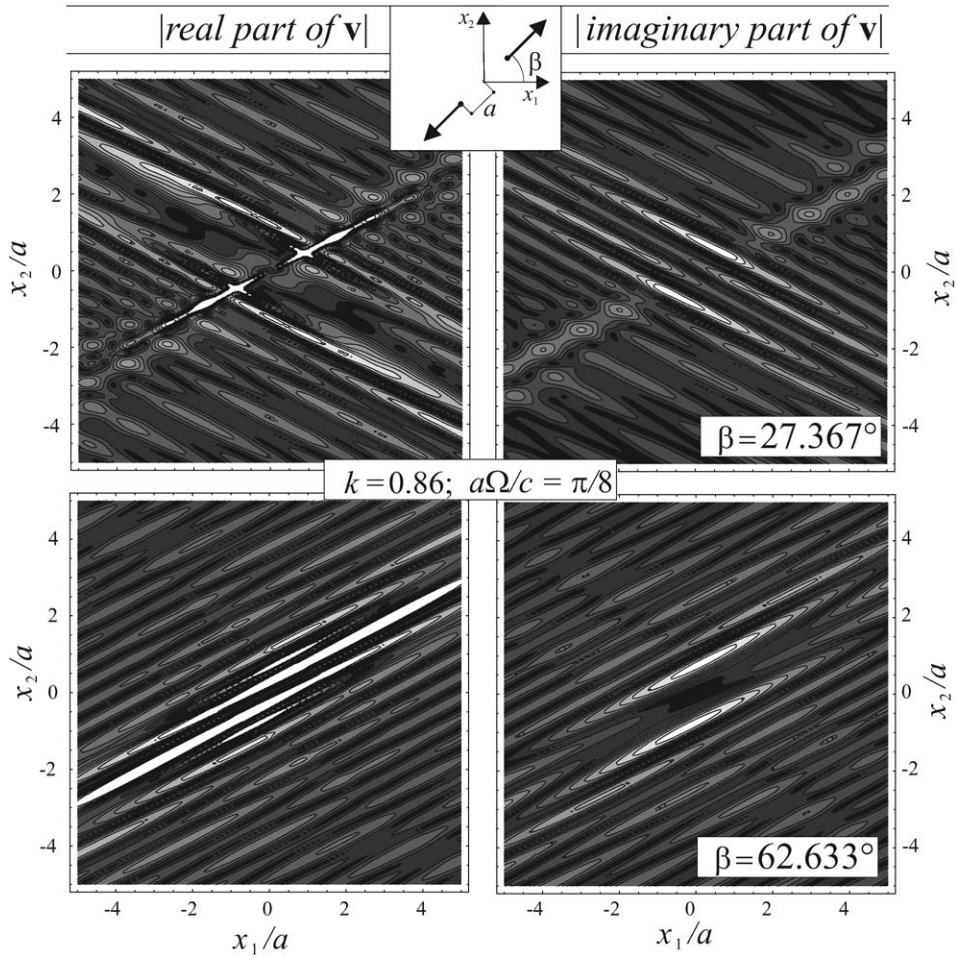


Fig. 8. Level sets of the modulus of the real part (left) and imaginary part (right) of incremental displacement, for a time-harmonic pulsating dipole inclined at angles 27.367° (upper part) and 62.633° (lower part) with respect to the x_1 -axis (i.e. the dipole is aligned parallel and orthogonal to the shear band evaluated at the elliptic boundary). An anisotropic material with $\mu_*/\mu = 1/4$ and a pre-stress $k = 0.86$ is considered near the boundary of ellipticity and $a\Omega/c = \pi/8$.

believe that the above approach opens a new perspective to the analyses of material instability.

5. Integral representations for time-harmonic dynamics

For incremental problems consisting of dynamic time-harmonic deformation superimposed upon a given homogeneous, pre-stressed (and equilibrated) state, it is possible to formulate integral representations for incremental displacements v_i and

in-plane hydrostatic stress \dot{p} . The procedure is strictly analogous to the quasi-static case for displacements, while it becomes substantially different for the hydrostatic stress and yields a generalization to the previous formulation given by [Bigoni and Capuani \(2002\)](#).

The importance of the boundary integral representations is that they provide (together with the obtained Green’s function set) the basis for boundary element methods in nonlinear elasticity, a possibility explored for the quasi-static case by [Bigoni and Capuani \(2002\)](#) and [Brun et al. \(2003a, b\)](#).

5.1. Boundary integral formulation for incremental displacements

Following the same procedure employed for the quasi-static case, but considering the equations pertinent to the time-harmonic dynamics, one obtains for the incremental displacement at point \mathbf{y} of a generic body

$$v_j(\mathbf{y})C_j^g = \int_{\partial B} [\dot{i}_{ij} n_i v_j^g(\mathbf{x} - \mathbf{y}) - \dot{i}_{ij}^g(\mathbf{x} - \mathbf{y}) n_i v_j] dl_x, \tag{43}$$

where ∂B denotes the boundary of the body with outer unit normal n_i ; v_i is the incremental displacement; \dot{i}_{ij} and \dot{i}_{ij}^g are the incremental nominal stresses, associated with v_i and v_i^g , respectively. Finally, the matrix C_j^g still has the same definition as in the quasi-static case, namely

$$C_j^g = \lim_{\varepsilon \rightarrow 0} \int_{\partial C_\varepsilon} \dot{i}_{ij}^g(\mathbf{x} - \mathbf{y}) n_i dl_x, \tag{44}$$

where C_ε is a disk of radius ε centred at \mathbf{y} . Since the dynamic Green’s function asymptotically reduces to the quasi-static one as $r \rightarrow 0$, the components of C_j^g are the same as in the quasi-static case. For points \mathbf{y} interior to the body, $C_j^g = \delta_{gj}$, while $C_j^g = \delta_{gj}/2$ at a smooth boundary point.

5.2. Boundary integral formulation for in-plane incremental hydrostatic stress

As for the quasi-static case ([Bigoni and Capuani, 2002](#)), to establish an integral representation for incremental hydrostatic stress we follow here a procedure which represents a generalization of the technique employed by [Ladyzhenskaya \(1963\)](#) for two-dimensional Stokes flow. In particular, a substitution of the constitutive equations (1) into the rate equations of (time-harmonic) motion gives

$$\dot{p}_{,h} = -\mathbb{K}_{ihkl} v_{l,ki} - \rho \Omega^2 v_h \tag{45}$$

which, used with the second gradient of Eq. (43) taken at interior points, yields

$$\dot{p}_{,h}(\mathbf{y}) = - \int_{\partial B} \mathbb{K}_{nhsg} [\dot{i}_{ij} n_i v_{j,sn}^g(\mathbf{x} - \mathbf{y}) - \dot{i}_{ij,sn}^g(\mathbf{x} - \mathbf{y}) n_i v_j] dl_x - \rho \Omega^2 v_h. \tag{46}$$

Noting that at interior points, $\mathbf{x} \neq \mathbf{y}$, the following relationship holds:

$$-\dot{p}_{,h}^j = \mathbb{K}_{nhsg} v_{j,sn}^g + \rho \Omega^2 v_h^j, \tag{47}$$

where

$$\dot{p}^g = \dot{\pi}^g + \frac{\sigma}{2} v_{1,1}^g. \tag{48}$$

Eq. (46) becomes

$$\begin{aligned} \dot{p}_{,h}(\mathbf{y}) &= \int_{\partial B} \dot{i}_{ig} n_i \dot{p}_{,h}^g(\mathbf{x} - \mathbf{y}) dl_x + \int_{\partial B} \mathbb{K}_{nhsq} \dot{i}_{ij,sn}^g(\mathbf{x} - \mathbf{y}) n_i v_j dl_x \\ &\quad + \rho \Omega^2 \int_{\partial B} \dot{i}_{ij}^h(\mathbf{x} - \mathbf{y}) n_i v_j dl_x, \end{aligned} \tag{49}$$

where $\dot{p}_{,h}^g$ is derived with respect to x_h . By means of a procedure similar to that employed for quasi-static deformation, the following expression for the gradient of the hydrostatic stress increment can be obtained at a point \mathbf{y} interior to the body

$$\begin{aligned} \dot{p}_{,h}(\mathbf{y}) &= \int_{\partial B} \dot{i}_{ig} n_i \dot{p}_{,h}^g(\mathbf{x} - \mathbf{y}) dl_x - \int_{\partial B} n_i v_j \mathbb{K}_{ijkq} \dot{p}_{,hk}^g(\mathbf{x} - \mathbf{y}) dl_x \\ &\quad + \int_{\partial B} v_i n_i \left[\left(4\mu\mu_* - 4\mu_*^2 + \sigma\mu - 2\mu_*\sigma - \frac{\sigma^2}{2} \right) v_{1,11}^1(\mathbf{x} - \mathbf{y}) \right. \\ &\quad \left. - \sigma \left(\mu + \frac{\sigma}{2} \right) v_{2,11}^2(\mathbf{x} - \mathbf{y}) \right]_{,h} dl_x \\ &\quad + \rho \Omega^2 \int_{\partial B} v_i n_i [a_h(\mathbf{x} - \mathbf{y}) + \dot{p}^h(\mathbf{x} - \mathbf{y})] dl_x, \end{aligned} \tag{50}$$

where

$$a_1 = 2(\mu - \mu_*)v_{1,1}^1 - \sigma(v_{1,1}^1 + v_{2,1}^2), \quad a_2 = 2(\mu - \mu_*)v_{2,2}^2. \tag{51}$$

Let us now take $\dot{f}_i = \delta_{ig}\delta(\mathbf{x})$ in Eqs. (6) written for the Green incremental displacement v_i^g and subtract the resulting Eq. (6)₂, with $g = 1$, from Eq. (6)₁, with $g = 2$. The following identity results

$$(a_1 + \dot{p}^1)_{,2} = (a_2 + \dot{p}^2)_{,1}, \tag{52}$$

showing that a potential $W(\mathbf{x} - \mathbf{y})$ can be introduced

$$W_{,h} = (a_h + \dot{p}^h), \tag{53}$$

so that Eq. (50) can be integrated with respect to y_h , yielding

$$\begin{aligned} \dot{p}(\mathbf{y}) &= - \int_{\partial B} \dot{i}_{ig} n_i \dot{p}^g(\mathbf{x} - \mathbf{y}) dl_x + \int_{\partial B} n_i v_j \mathbb{K}_{ijkq} \dot{p}_{,k}^g(\mathbf{x} - \mathbf{y}) dl_x \\ &\quad - \int_{\partial B} v_i n_i \left[\left(4\mu\mu_* - 4\mu_*^2 + \sigma\mu - 2\mu_*\sigma - \frac{\sigma^2}{2} \right) v_{1,11}^1(\mathbf{x} - \mathbf{y}) \right. \\ &\quad \left. - \sigma \left(\mu + \frac{\sigma}{2} \right) v_{2,11}^2(\mathbf{x} - \mathbf{y}) + \rho \Omega^2 W(\mathbf{x} - \mathbf{y}) \right] dl_x, \end{aligned} \tag{54}$$

where $\dot{p}_{,k}^g$ is differentiated with respect to x_k . It is worth noting that the fact that the signs of Eq. (54) are opposite to those appearing in Eq. (50) is a consequence of integration with respect to \mathbf{y} . Eq. (54) is an integral equation relating the in-plane

hydrostatic stress increment at interior points of the body to the boundary values of nominal traction and displacement increments. Note that the term W contained in Eq. (54) (and which is absent in the quasi-static counterpart) is not null even under the assumption of isotropy, $\mu = \mu_*$, and null pre-stress, $k = 0$. Moreover, the fact that the potential W is defined modulo an arbitrary constant does not affect the boundary integral equation (54) since the flux of velocity v_i through any closed surface is null as a consequence of incompressibility.

To make Eq. (54) explicit, the expression for the potential W must be obtained. Let us begin observing that it follows from Eq. (53) that

$$W_{,1} + W_{,2} = 2(\mu - \mu_*)(v_{1,1}^1 + v_{2,2}^2) - \sigma(v_1^1 + v_2^2)_{,1} + \dot{p}^1 + \dot{p}^2. \tag{55}$$

Taking the plane wave expansion of function W

$$W = -\frac{1}{4\pi^2} \oint_{|\omega|=1} \tilde{W}(\omega \cdot \mathbf{x}) d\omega. \tag{56}$$

Eq. (55) can be re-written as

$$(\omega_1 + \omega_2)\tilde{W}' = 2(\mu - \mu_*)(\omega_1\tilde{v}_1^1 + \omega_2\tilde{v}_2^2)' - \sigma\omega_1(\tilde{v}_1^1 + \tilde{v}_2^2)' + \tilde{p}^1 + \tilde{p}^2. \tag{57}$$

Employing the incompressibility condition and the symmetry property $v_2^1 = v_1^2$, Eq. (57) can be integrated leading to

$$\tilde{W} = [4(\mu - \mu_*)\omega_2^2 - \sigma]\tilde{v}_2^2(\omega \cdot \mathbf{x}) + \log |\omega \cdot \mathbf{x}|, \tag{58}$$

where $\tilde{v}_2^2(\omega \cdot \mathbf{x})$ is given by Eq. (29).

Finally, Eq. (58) through Eq. (55) provides the potential W to be employed in the boundary integral equation (54)

$$\begin{aligned} W(r, \vartheta) &= -\frac{1}{2\pi} \log \frac{\Omega r}{c} - \frac{1}{2\pi^2 \mu(1+k)} \\ &\times \left[\left(\log \left(\frac{\Omega r}{c} \right) + \gamma \right) \int_0^\pi \frac{4(\mu - \mu_*)\sin^2(\alpha + \vartheta) - \sigma}{\Lambda(\alpha + \vartheta)} \cos^2(\alpha + \vartheta) \right. \\ &\times \cos \left(\frac{\Omega r}{c} \frac{\cos \alpha}{\sqrt{\Lambda(\alpha + \vartheta)}} \right) d\alpha + \int_0^{\pi/2} \frac{4(\mu - \mu_*)\sin^2(\alpha + \vartheta) - \sigma}{\Lambda(\alpha + \vartheta)} \\ &\times \cos^2(\alpha + \vartheta) \log \left(\frac{\cos \alpha}{\sqrt{\Lambda(\alpha + \vartheta)}} \right) \cos \left(\frac{\Omega r}{c} \frac{\cos \alpha}{\sqrt{\Lambda(\alpha + \vartheta)}} \right) d\alpha \\ &\left. + \int_0^{\pi/2} \frac{4(\mu - \mu_*)\cos^2(\alpha + \vartheta) - \sigma}{\Lambda(\alpha + \vartheta + \pi/2)} \sin^2(\alpha + \vartheta) \log \left(\frac{\sin \alpha}{\sqrt{\Lambda(\alpha + \vartheta + \pi/2)}} \right) \right] \end{aligned}$$

$$\begin{aligned}
& \times \cos\left(\frac{\Omega r}{c} \frac{\sin \alpha}{\sqrt{\Lambda(\alpha + \vartheta + \pi/2)}}\right) d\alpha + \int_0^\pi \frac{4(\mu - \mu_*)\sin^2(\alpha + \vartheta) - \sigma}{\Lambda(\alpha + \vartheta)} \\
& \times \cos^2(\alpha + \vartheta) \Im\left(\frac{\Omega r}{c} \frac{\cos \alpha}{\sqrt{\Lambda(\alpha + \vartheta)}}\right) d\alpha - i \frac{\pi}{2} \int_0^\pi \frac{4(\mu - \mu_*)\sin^2(\alpha + \vartheta) - \sigma}{\Lambda(\alpha + \vartheta)} \\
& \times \cos^2(\alpha + \vartheta) \cos\left(\frac{\Omega r}{c} \frac{\cos \alpha}{\sqrt{\Lambda(\alpha + \vartheta)}}\right) d\alpha \Big]. \tag{59}
\end{aligned}$$

Since the potential W is defined modulo an arbitrary constant, we note that the term $\log(\Omega r/c)$ in Eq. (59) can be replaced by $\log \hat{r}$, with \hat{r} denoting any dimensionless measure of distance. In the particular case of isotropy, $\mu = \mu_*$, and null pre-stress, $k = 0$, W reduces to $-\log(\Omega r/c)/(2\pi)$ and the boundary integral equation (54) with W given by Eq. (59) boils down to that provided by [Polyzos et al. \(1998\)](#) and, in the quasi-static limit ($\rho\Omega \rightarrow 0$), to that obtained by [Ladyzhenskaya \(1963\)](#).

6. Conclusions

Time-harmonic dynamics of incremental nonlinear and incompressible elastic deformations superimposed upon an arbitrary but homogeneous strain has been considered. The infinite-body Green's function set has been determined together with boundary integral equations for incremental displacements and hydrostatic stress. These results provide the basis for boundary element techniques in dynamic, nonlinear elasticity.

Employed as a dynamic perturbation, the Green's function has revealed features of signal propagation in a solid stretched until near the boundary of loss of ellipticity. Here the propagation becomes highly localized along directions corresponding to the shear band inclinations found in the quasi-static limit. Even though this might have been anticipated, the analytical determination of dynamic deformation maps provides a new point of view, which for example may help in the design of filters for mechanical waves. Results presented in this paper demonstrate that the proposed perturbative approach may become effective when employed in, say, "nonstandard situations". In particular, we believe that the proposed technique can be extended to a broad range of contexts, involving dynamics (for instance in the analysis of flutter instability in a continuous medium ([Piccolroaz et al., 2004](#))), non-homogeneity (for instance shear bands formation in a non-uniform material) and temperature effects (for instance analysis of adiabatic vs. isothermal shear banding).

Acknowledgements

D.B. gratefully acknowledges financial support from MURST-Cofin 2004 (Microstructural problems and models: applications in structural and civil

engineering); D.C. thanks financial support from MURST-Cofin 2002 (2002084245_004).

References

- Bigoni, D., Capuani, D., 2002. Green's function for incremental nonlinear elasticity: shear bands and boundary integral formulation. *J. Mech. Phys. Solids* 50, 471–500.
- Bigoni, D., Petryk, H., 2002. A note on divergence and flutter instabilities in elastic–plastic materials. *Int. J. Solids Struct.* 39, 911–926.
- Biot, M.A., 1965. *Mechanics of Incremental Deformations*. Wiley, New York.
- Brun, M., Capuani, D., Bigoni, D., 2003a. A boundary element technique for incremental, nonlinear elasticity. Part I: Formulation. *Comput. Methods Appl. Mech. Eng.* 192, 2461–2479.
- Brun, M., Bigoni, D., Capuani, D., 2003b. A boundary element technique for incremental, nonlinear elasticity. Part II: Bifurcation and shear bands. *Comput. Methods Appl. Mech. Eng.* 192, 2481–2499.
- Gel'fand, I.M., Shilov, G.E., 1964. *Generalized Functions*, vol. 1, Properties and Operations. Academic Press, New York.
- Knowles, J.K., Sternberg, E., 1978. On the failure of ellipticity and the emergence of discontinuous deformation gradients in plane finite elastostatics. *J. Elast.* 8, 329–379.
- Ladyzhenskaya, O.A., 1963. *The Mathematical Theory of Viscous Incompressible Flow*. Gordon and Breach, New York.
- Merodio, J., Ogden, R.W., 2002. Material instabilities in fiber-reinforced nonlinearly elastic solids under plane deformation. *Arch. Mech.* 54, 525–552.
- Merodio, J., Pence, T.H., 2001. Kink surfaces in a directionally reinforced neo-Hookean material under plane deformation: I Mechanical equilibrium. *J. Elast.* 62, 119–144.
- Piccolroaz, A., Bigoni, D., Willis, J.R., 2005. A dynamical interpretation of flutter instability in a continuous medium, submitted for publication.
- Polyzos, D., Tsinopoulos, S.V., Beskos, D.E., 1998. Static and dynamic boundary element analysis in incompressible linear elasticity. *Eur. J. Mech. A/Solids* 17, 515–536.
- Renardy, M., Rogers, R.C., 1993. *An Introduction to Partial Differential Equations*. Springer, New York.
- Willis, J.R., 1973. Self-similar problems in elastodynamics. *Philos. Trans. R. Soc. London Ser. A* 274, 435–491.
- Willis, J.R., 1991. Inclusions and cracks in constrained anisotropic media. In: Wu, J.J., Ting, T.C.T., Barnett, D.M. (Eds.), *Modern Theory of Anisotropic Elasticity and Applications*. SIAM, Philadelphia, pp. 87–102.